Surface Photovoltage, Luminescence, and Cyclic Voltammetry on the First Series of Lanthanide(III) Monobenzoporphyrin Compound Liquid Crystals and Relative Transition Metal Benzoporphyrin Compound Liquid Crystals

Ming-Hui Qi and Guo-Fa Liu*

Department of Chemistry, Jilin University, Changchun 130023, People's Republic of China

Received: January 17, 2003; In Final Form: April 29, 2003

The first series of lanthanide(III) monobenzoporphyrin liquid crystalline compounds, *meso*-tetraalkyltetrabenzoporphyrin (TATBP) ytterbium hydroxy, and relative transition metal benzoporphyrin liquid crystalline compounds (4 series, 24 kinds) are reported that display a hexagonal columnar discotic columnar (Col_h, previously designated D_h) phase. These liquid crystalline compounds have been studied by cyclic voltammetry, luminescence, and surface photovoltage spectroscopies. In a dimethylformamide (DMF) solution of 0.1 M tetrabutylammonium perchlorate (TBAP), the synthesized TATBP and TATBPZn exhibit two one-electron reversible redox reactions, and TATBPYbOH and TATBPCoCl show three redox reactions, respectively, within the accessible potential window of the solvent and the measured electrochemical redox potentials. The absorption bands of the porphyrins appear in the ranges 425−438 (Soret band), 572−581 (Q-band), and 625−631 (Q-band) nm. The photovoltaic properties and charge-transfer process of the liquid crystalline compounds were investigated by surface photovoltage spectroscopy (SPS) and electric-field-induced surface photovoltage spectroscopy (EFISPS) techniques, which reveal that all compounds are P-type semiconductors. The spectral bands of TATBP and metal TATBP correspond to the $\pi \rightarrow \pi^*$ transition, and the metal ion corresponds to the π^* orbital ($d \rightarrow e_g(\pi^*)$) transition, respectively. The electron (or hole) can be trapped on the liquid crystal porphyrin film by applying both light and a negative (or positive) electric field. Quantum yields of the $S_1 \rightarrow S_0$ fluorescence are in the region 0.20−0.28, and the fluorescence lifetimes are in the region 0.015−0.028 ms at room temperature. The phosphorescence bands of the complexes at 77 K appear in the range 715−725 nm. It is found that the stronger the fluorescence intensity is, the weaker the surface photovoltage intensity is. The TATBPCo(III)Cl are 1:1 type electrolytes. The study contributes to further choice and applications of the liquid crystals.

1. Introduction

Porphyrin liquid crystals[1,2] are of interest for optoelectronic and other device applications due to their synthetic versatility, thermal stability, large π-electron systems, and photochemical properties.[3] The studies of previously reported liquid crystal compounds concentrated mainly upon liquid crystallinity, or a certain aspect property such as fluorescence.[4] We comprehensively study photochemical hole-burning, semiconductor, and luminescence properties of the first series of lanthanide(III) monobenzoporphyrin compound liquid crystals and relative transition metal benzoporphyrin compound liquid crystals by cyclic voltammetry, surface photovoltage, and luminescence spectroscopies. To date, few of the aspects had been reported.

The surface photovoltage spectroscopy (SPS) technique, as a very sensitive characterization method which detects the change of charge distribution on a functional semiconductor surface, not only is related to the electron transition process caused by light absorption but also reflects directly the properties of photogenerated charge separation and charge transfer. Its sensitivity comes to 10^8 q/cm^2, which exceeds that of such conventional spectroscopies as XPS and Auger spectroscopy by many orders of magnitude.[5]

These studies will provide wider ground for choice and applications of the materials.

* E-mail: minghuiqi@yahoo.com.

2. Results and Discussion

2.1. Liquid Crystals. The structures of these compounds are shown in Figure 1. The liquid crystalline phases of all compounds were characterized by differential scanning calorimetry (DSC), and the characterization was confirmed by viewing the birefringence of the samples between crossed polarizers in a polarizing microscope. The DSC results of TATBPYbOH (*meso*-tetraalkyltetrabenzoporphyrin = TATBP) are summarized in Figure 2. The peak corresponding to the liquid crystal to solid phase transition was large and sharpened with the alkyl chain length increase. The peak from isotropic liquid to liquid crystal phase was somewhat broad in all samples. The liquid crystal to solid phase enthalpy decreased with increasing alkyl chain length (from −3.5 kJ/mol for R═C_6H_{13}-YbOH to −10.7 kJ/mol for R═$C_{16}H_{33}$YbOH for the cooling cycle), although the enthalpy of the isotropic liquid to liquid crystal phase transition increased (from −11.0 kJ/mol for R═C_6H_{13}YbOH to −3.5 kJ/mol for R═$C_{16}H_{33}$YbOH for the cooling cycle). The results of the other three series of compounds (Table 1) are similar to those of TATBPYbOH. All compounds are liquid crystals at room temperature.

The single liquid crystalline domains on the order of 20−45 μm for all of the mesogenic samples were obtained by annealing them from their clearing temperature. Figure 3 shows two examples of the birefringence texture for 14Zn and 14L. Due to alignment of the molecules with the polarizer and the

10.1021/jp034128p CCC: $25.00
Published on Web 07/02/2003

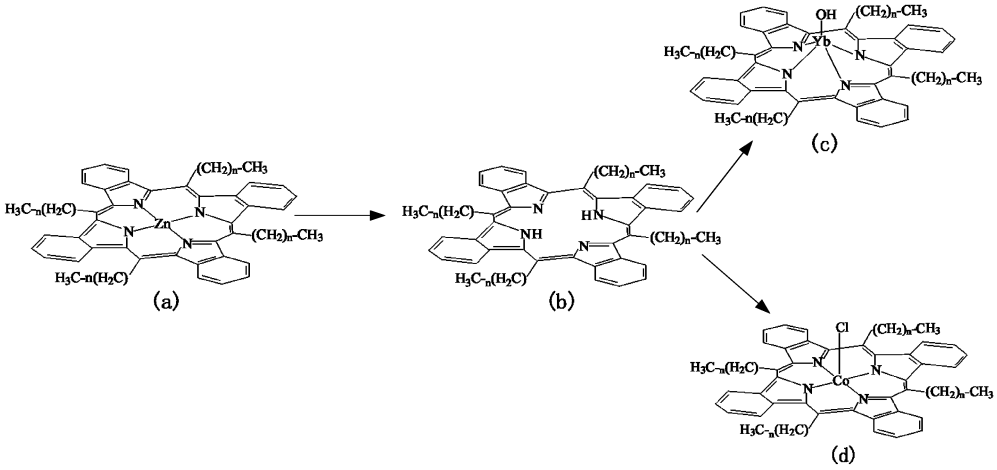

Figure 1. Hexagonal columnar benzoporphyrin liquid crystalline compounds: (a) tetraalkyltetrabenzoporphyrin zinc(II) (TATBPZn), $n = 5$, 7, 9, 11, 13, and 15 correspond to 6Zn, 8Zn, 10Zn, 12Zn, 14Zn, and 16Zn, respectively; (b) tetraalkyltetrabenzoporphyrin (TATBP), $n = 5$, 7, 9, 11, 13, and 15 correspond to 6L, 8L, 10L, 12L, 14L, and 16L, respectively; (c) tetraalkyltetrabenzoporphyrin ytterbium(III) hydroxy (TATBPYbOH), $n =$ 5, 7, 9, 11, 13, and 15 correspond to 6YbOH, 8YbOH, 10YbOH, 12YbOH, 14YbOH, and 16YbOH, respectively; (d) tetraalkyltetrabenzoporphyrin cobalt(III) (TATBPCoCl), $n = 5$, 7, 9, 11, 13, and 15 correspond to 6CoCl, 8CoCl, 10CoCl, 12CoCl, 14CoCl, and 16CoCl, respectively.

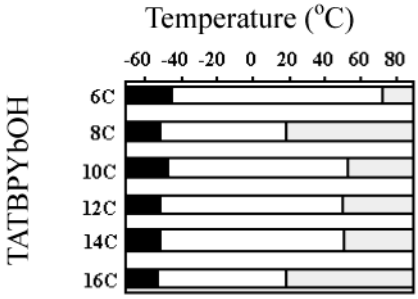

Figure 2. Differential scanning calorimetry of the TATBPYbOH: black = solid phase; white = mesophase; gray = isotropic phase. The DSC peak maxima for the cooling cycle (10 °C/min) are as follows [temperature (ΔH); M = transition of mesophase to solid, C = transition of isotropic to mesophase]: C_6 [−44.1 °C (−3.5 kJ/mol) M, 72.5 °C (−11.0 kJ/mol) C]; C_8 [−50.0 °C (−7.1 kJ/mol) M, 19.2 °C (−10.8 kJ/mol) C]; C_{10} [-46.5 °C (−8.2 kJ/mol) M, 54.8 °C (−9.5 kJ/mol) C]; C_{12} [−51.5 °C (12.2 kJ/mol) M, 51.1 °C (−8.8 kJ/mol) C]; C_{14} [−51.4 °C (−14.4 kJ/mol) M, 50.0 °C (−8.5 kJ/mol) C]; C_{16} [−52.3 °C (−10.7 kJ/mol) M, 19.1 °C (−3.5 kJ/mol) C].

TABLE 1: Phase Transition Temperatures and Enthalpy Changes of the Porphyrin Derivatives

compd	phase[a]	T/°C (ΔH/kJ·mol^{-1})	phase[a]	T/°C (ΔH/kJ·mol^{-1})	phase[a]
6Zn	C	−20.8 (−0.7)	D	73.4 (−7.3)	I
8Zn	C	−51.8 (−10.8)	D	24.4 (−2.5)	I
10Zn	C	−20.6 (−0.9)	D	56.4 (−5.6)	I
12Zn	C	−20.5 (−1.2)	D	50.4 (−3.5)	I
14Zn	C	−20.5 (−10.5)	D	50.8 (−1.6)	I
16Zn	C	−21.0 (−20.6)	D	48.8 (−0.9)	I
6L	C	−42.6 (−0.8)	D	74.2 (−7.9)	I
8L	C	−50.6 (−11.0)	D	26.5 (−0.1)	I
10L	C	−44.9 (−1.4)	D	55.6 (−4.6)	I
12L	C	−46.6 (−8.5)	D	52.6 (−4.3)	I
14L	C	−49.9 (−9.1)	D	51.3 (−2.5)	I
16L	C	−52.3 (−12.7)	D	22.3 (−3.8)	I
6CoCl	C	−42.5 (−2.6)	D	75.2 (−15.6)	I
8CoCl	C	−50.2 (−5.1)	D	25.6 (−12.0)	I
10CoCl	C	−46.5 (−8.2)	D	55.5 (−9.8)	I
12CoCl	C	−48.9 (−10.8)	D	50.7 (−6.9)	I
14CoCl	C	−50.8 (−14.5)	D	51.6 (−4.5)	I
16CoCl	C	−52.2 (−16.8)	D	17.5 (−1.4)	I

[a] C, crystal; D, discotic mesophase; I, isotropic liquid.

analyzer, a classic Maltese cross[6] (Figure 3a) extinction pattern was observed in the polarizer direction (vertical in the figure) and analyzer direction (horizontal in the figure).

Small-angle X-ray scattering (SAXS) of 14YbOH at 25 °C shows reflections with d spacings of 41.4 and 24.2 Å, which correspond to the first two reflections of a hexagonal columnar structure (reciprocal d spacing of $1:\sqrt{3}$). We conclude that the mesophase structure is probably a hexagonal columnar discotic columnar, Col_h (previously designated D_h).[7] Wide-angle X-ray diffraction gave one broad peak, which is centered at 4.6 Å, that is due to the commonly seen liquidlike packing of alkyl chains in the mesophase. The X-ray scattering results of other compounds are similar to those of 14YbOH; therefore, their mesophase structures are all Col_h.

2.2. Electrochemistry. Cyclic voltammetric studies have been performed to evaluate the redox potentials. Within the accessible potential window of the solvent, two reversible redox processes of 14L and 14Zn in 0.1 M tetrabutylammonium perchlorate (TBAP) in DMF have been observed, respectively, and three of 14YbOH and 14CoCl are so. The first and second redox potentials corresponding to the benzoporphyrin ring reaction of 14L and 14Zn are located at $E_{1/2} = -1.456$, -2.276 and -1.436, -2.114 V vs Ag/Ag$^+$, respectively.[8] The corresponding potentials for the benzoporphyrin ring reaction of 14YbOH are located at $E_{1/2} = -1.445$ and -2.253 V vs Ag/Ag$^+$, respectively. The third redox potentials of 14YbOH concerning lanthanide metal (ytterbium) ion are located at $E_{1/2} = -2.388$ V vs Ag/Ag$^+$. However, the redox reaction in 14CoCl differs markedly from that in the other porphyrins. That is, the corresponding benzoporphyrin ring reduction potentials are the third redox potentials and are located at $E_{1/2} = -2.204$ V vs Ag/Ag$^+$, while the potentials for cobalt(III) ion reduction are the first and second redox potentials and are located at $E_{1/2} = -1.425$ and -2.047 V vs Ag/Ag$^+$, respectively.[8] Comparing the cyclic voltammetric results of 14L, 14Zn, 14YbOH, and 14CoCl, it is found that the redox potentials reveal that negative shift increased in the order 14CoCl, 14Zn, 14YbOH, and 14L. This is probably due to different atomic radii; the bigger the atomic radius is, the easier the loss of the electron is. These results collectively indicate that the reducing property of the complexes is very strong. There are similar results for the samples whose central ions are identical with those above.

2.3. Absorption Spectra. Characteristic Q and B (Soret) bands of metal porphyrin in visible and near-ultraviolet ranges are assigned as the transitions from the ground state (S_0) to the

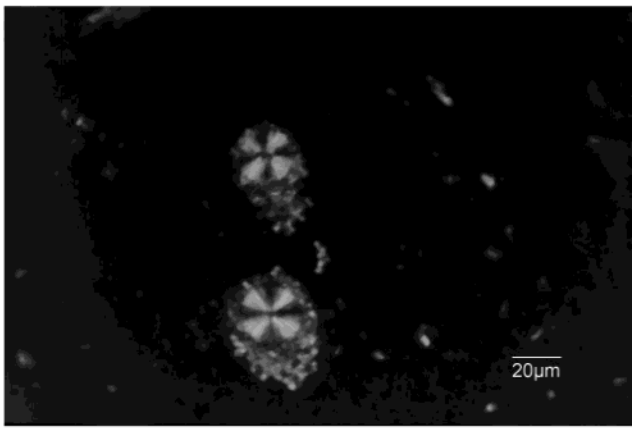

(a)

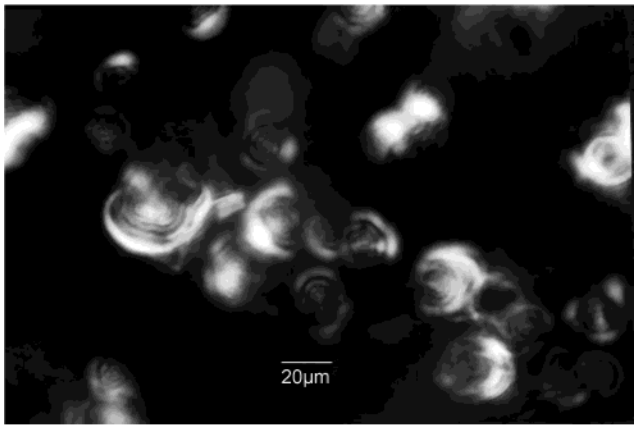

(b)

Figure 3. Birefringence texture micrograph of 14Zn and 14L viewed between crossed polarizers. The domains were grown from the isotropic phase to 25 °C as the sample was being annealed: (a) 14Zn; (b) 14L.

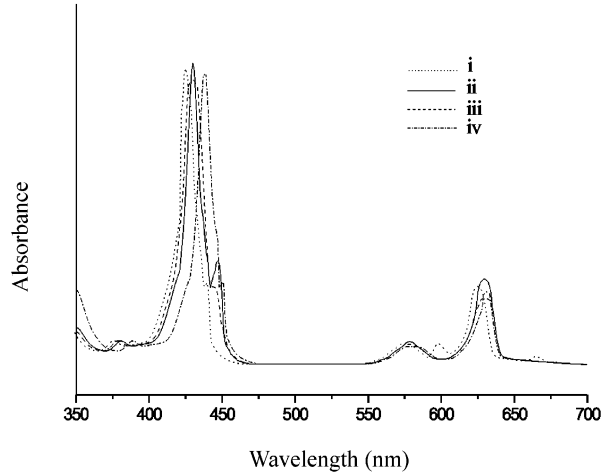

Figure 4. UV/vis spectra of (i) 14L, (ii) 14Zn, (iii) 14CoCl, and (iv) 14YbOH taken in a solution of $CHCl_3$.

lowest excited singlet (S_1) and the second excited singlet states (S_2), respectively. Figure 4 shows absorption spectra of 14L, 14Zn, 14CoCl, and 14YbOH.

The absorption bands of the free base 14L appear at 425 (Soret), 576 (Q), 601 (Q), 625 (Q), and 665 (Q) nm, and those of the complexes appear in the regions 430−438 (soret), 578−580 (Q), and 629−631 (Q) nm. Compared with the case of the ligand 14L, the number of the absorption bands of the complexes decreases, which is due to the symmetry increase of the

TABLE 2: Absorption Spectral Maxima (nm)[a]

porphyrin	B (Soret)	Q			
14L	425	576	601	625	665
	(2.3×10^5)	(3.2×10^4)	(3.6×10^4)	(5.7×10^4)	(2.9×10^4)
14Zn(II)	430	578		629	
	(2.2×10^5)	(3.6×10^4)		(5.6×10^4)	
14Co(III)Cl	430	578		630	
	(2.2×10^5)	(2.9×10^4)		(5.7×10^4)	
14Yb(III)OH	438	580		631	
	(2.2×10^5)	(3.2×10^4)		(5.8×10^4)	

[a] In chloroform at room temperature. Molar extinction coefficients are in parentheses.

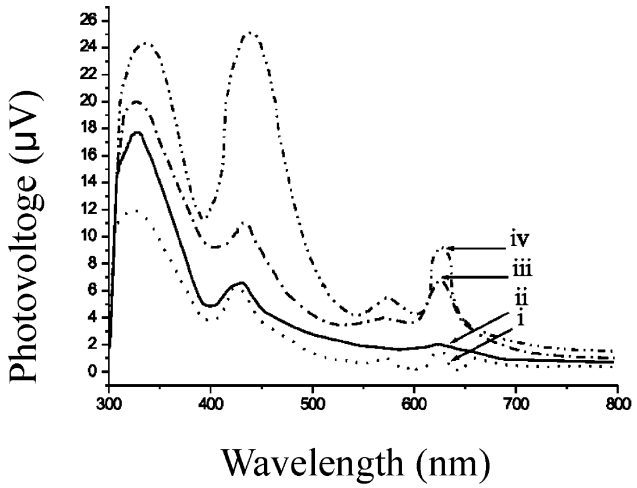

Figure 5. Surface photovoltage spectra of (i) 14L, (ii) 14Zn, (iii) 14CoCl, and (iv) 14YbOH thin films without an external field.

complexes, and absorption bands exhibit a small shift to longer wavelengths; however, those of rare earth complexes have a larger shift. The intensity and maxium absorption wavelengths (λ_{max}) of the complexes for Q bands are much less sensitive to the central metal ion and axial ligands; however, those of the complexes for the B (soret) band are sensitive to the central metal ion and axial ligands (Table 2).

2.4. Surface Photovoltage Spectroscopy. Benzoporphyrins, as π-conjugated systems of enlargement, have obvious organic semiconducting characteristics. The bonding π orbital is analogous to the valence band, and the antibonding one, to the conduction band. Photogenerated charge carriers in the π system are nonlocalized; their motion is free within the energy band of the π system. Photogenerated holes move in the valence band, and photogenerated electrons, in the conduction band. For this kind of system, the band to band transition is characterized as a $\pi \rightarrow \pi^*$ transition exhibiting chiefly Soret and Q bands. Figure 5 shows the photovoltage response of 14L, 14Zn, 14CoCl, and 14YbOH in the region 300−670 nm; the Soret band manifests a strong positive photovoltage response.

The signal detected by surface photovoltage spectroscopy (SPS) is equivalent to the change in the surface potential barrier on illumination: $\delta V = V_s' - V_s^\circ$,[9] where V_s' and V_s° are the surface potential heights before and after illumination, respectively. As far as band to band transitions are concerned, a positive response of surface photovoltage (SPV) ($\delta V > 0$) means that the sample is characterized as a p-type semiconductor. The photoinduced charge transfer, electron−hole separation, and change of V_s in p-type semiconductors[9] are shown in Figure 6. E_c, E_v, and E_f are the minimum energy of the conduction band, the maximum energy of the valence band, and the Fermi level energy, respectively. E_m is the occupied orbital, and E_g is the forbidden bandwidth. It illustrates the charge-transfer process

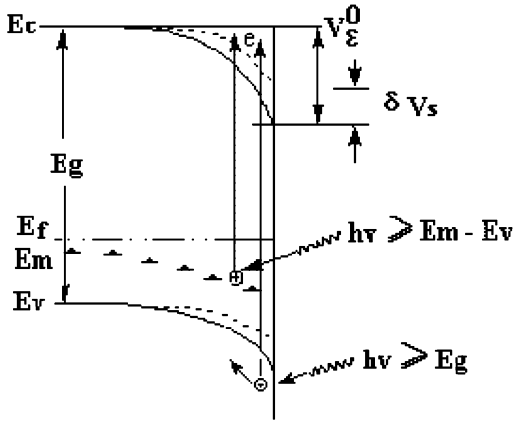

Figure 6. Photoexcitation and photogenerated charge-transfer process in the compounds.

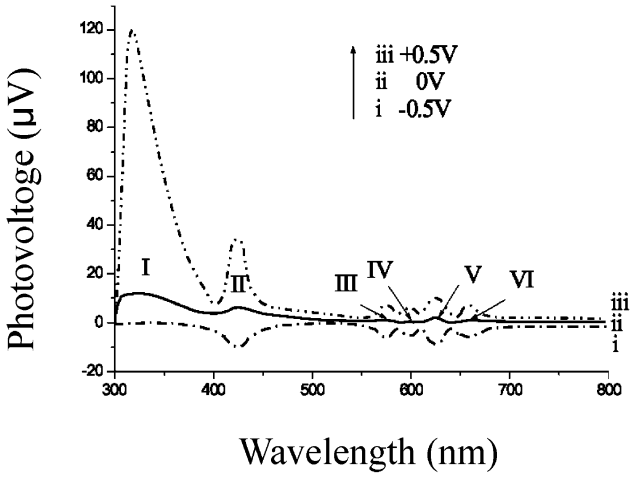

Figure 7. Surface photovoltage spectra of 14L thin films under positive and negative external fields. I, II, III, IV, V, and VI correspond to the six peaks of 14L, respectively.

with a positive SPV response. Band to band transitions occur when $h\nu \geq E_g$; electrons are excited to the conduction band, while holes are left in the valence band. Under the action of the built-in field, holes in the valence band move toward the bulk, while electrons in the conduction band diffuse to the surface, resulting in a net positive charge in the space-charge region; band bending decreases and δV_s is positive. These samples are all p-type semiconductors.

2.5. Electric-Field-Induced Surface Photovoltage Spectroscopy. The SPV response of 14L with different external electric fields is given in Figure 7. Comparing the spectral peaks, it is found that there is a "simultaneous response" with a change in the positive or negative electric field intensity. The SPV response is positive in a positive electric field but negative in a negative electric field. A simultaneous response to the electric field indicates that P_I-P_{IV} can all be assigned to $\pi \rightarrow \pi^*$ transitions. However, the variation rates of P_I and P_{II} with an increase in the positive or negative electric field intensity are noticeably different. A large positive increase in the SPV response with positive electric field is observed for P_I, while P_{II} exhibits a fast negative increase along the negative direction. Because the common upper energy level transition in the π system is toward $e_g(\pi^*)$, the difference stems from the lower energy levels. This phenomenon shows that the lower energy levels of these transitions are at different depths from the valence band, indicating different photogenerated hole diffusion lengths.

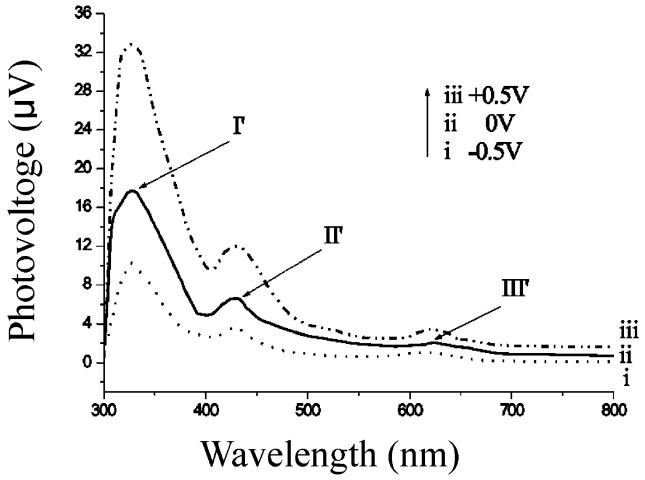

Figure 8. Surface photovoltage spectra of 14Zn thin films under positive and negative external fields.

The response of the Q band is induced in a positive electric field. Consistent with the Soret band, this is due to the fact that the external electric field reduces the recombination rate of photogenerated charges and prolongs the lifetime of the excited state.

The SPV response of 14Zn is shown in Figure 8. Although the intensities of $P_I'-P_{III}'$ are different, their responses to the external electric field are similar. This indicates that these transitions are identical. $P_I'-P_{III}'$ is positive without an external electric field, increases with a positive external electric field, and decreases with a negative external electric field. Comparing Figures 8 and 7, it is found that the SPV response of 14Zn is different from that of 14L, which shows no symmetrical reversal with positive or negative fields, and those exhibit also no negative value. This indicates that $P_I'-P_{III}'$ cannot be attributed to $\pi \rightarrow \pi^*$ transitions or LMCT (from ligand to metal charge transfer) transitions. The photovoltaic process of 14Zn can be illustrated using Figure 6. E_m may be the energy of d_{z^2}, d_{xz}, d_{yz}, and d_{xy}. After illumination ($h\nu > E_c - E_m$), the electrons in these energy levels are excited to the conduction band (π^*) and localized positive charges are produced on E_m. Due to the influence of the built-in field, electrons in the conduction band diffuse to the surface, resulting in excess positive charge in the space-charge region and a positive SPV response. With a positive electric field, the built-in field is enhanced, increasing the diffusion length of electrons in the conduction band, more electrons reach the surface, and the response of $P_I'-P_{III}'$ increases. With a negative electric field, electrons in the conduction band move toward the bulk, partly neutralizing the positive charge on E_m, and therefore, the SPV response decreases. Results of electric-field-induced surface photovoltage spectroscopy (EFISPS) and photovoltaic experiments indicate that $P_I'-P_{III}'$ can be attributed to a transition from the d orbit of the Zn(II) ion to the π^* orbit of the porphyrin. The transition is therefore a metal to ligand charge transfer (MLCT) transition. Energetically, peak P_I' corresponds to a $d_{z^2} \rightarrow e_g(\pi^*)$ transition, peak P_{II}' corresponds to d_{xz}, $d_{yz} \rightarrow e_g(\pi^*)$ transition, while P_{III}' corresponds to a $d_{xy} \rightarrow e_g(\pi^*)$ transition. According to the above interpretation, the charge-transfer processes and absorption bands of 14Zn and 14L are illustrated in Figure 9. The transitions of 14YbOH and 14CoCl are similar to that of 14Zn.

When a positive electric field is applied, the electric field reduces the recombination rate of photogenerated charges and prolongs the lifetime of the excited state, leading to an increase

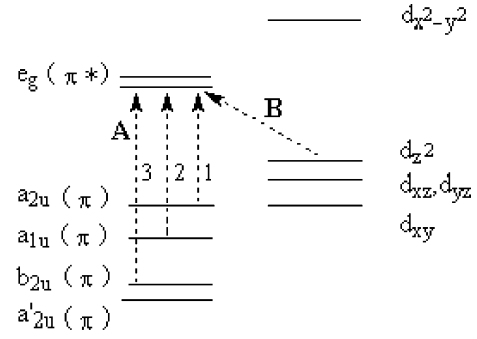

Porphyin	Metal(Zn^{2+})
A = (π → π *)	1.Q band
B = MLCT (d→ π *)	2. Soret band
	3. P_I band

Figure 9. Molecular level diagram and absorption band assignment for 14L and 14Zn.

TABLE 3: Excitation Spectral Maxima

porphyrin	*T*/K	maxima (λ_{max}/nm)				
14L	300	426	577	602	626	666
	77	433	584	609	633	673
14Zn(II)	300	431	579		630	
	77	438	586		637	
14Co(III)Cl	300	431	580		631	
	77	437	586		637	
14Yb(III)OH	300	440	582		633	
	77	446	588		639	

in the SPV response. With a negative electric field, the photogenerated electrons in the conduction band diffuse toward the bulks, which increases the probability of recombination with photogenerated holes whose diffusion lengths are shorten, leading to a decrease of the response.

The dependence of photovoltage for 14L on the applied voltage is almost symmetric for the positive and negative field. This interesting result is analogous to the electro-optical memory effect observed by Bard et al.[10] According to the experimental results of Bard et al., the electron (or hole) can be trapped on the liquid crystal porphyrin film by applying both light and negative (or positive) electric field. Our results confirm that photogenerated electrons (holes) are trapped in the sample under the positive (negative) field, and the left photogenerated holes create surface photovoltage.

2.6. Luminescence Spectra. Figure 10a shows the excitation spectra of 14L, 14Zn, 14CoCl, and 14YbOH at room temperature in chloroform. The emission spectra of these compounds at low temperature in chloroform are shown in Figure 10b. Spectral decay lifetimes and quantum yields of fluorescent emission were measured. Table 3 gives the excitation spectral maxima of these compounds.

There are fluorescences of the S_2 (B band) and the S_1 (Q band) in porphyrin complexes. The fluorescence of the B (Soret) band is attributed to the transition from the second excited singlet state S_2 to the ground state S_0, $S_2 \rightarrow S_0$. The Soret fluorescence is about 2 orders of magnitude weaker than that of the $S_1 \rightarrow S_0$ transition of the Q band emission. Its quantum yield is so low that sometimes fluorescence becomes unobservable. The quantum yields ϕ_f of the $S_1 \rightarrow S_0$ fluorescence of the porphyrins are in the region 0.20−0.28 (Table 4), which are essentially consistent with those of zinc tetrabenzoporphyrin (ZnTBP)[11] and meso-substituted-phenyl-zinc tetrabenzoporphyrins (ZnSPTBP).[12] They are higher much than those of TPPEr (dpm),[13]

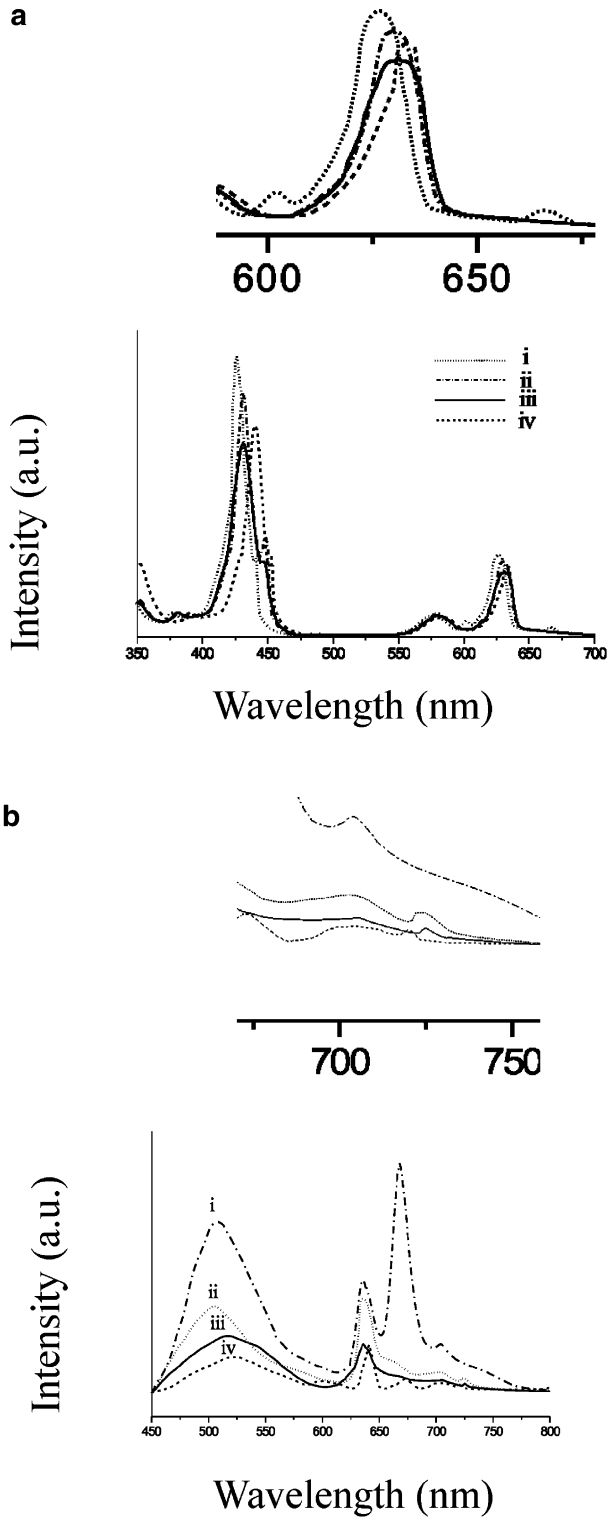

Figure 10. (a) Excitation spectra of (i) 14L, (ii) 14Zn, (iii) 14CoCl, and (iv) 14YbOH at room temperature in $CHCl_3$. (b) Fluorescence spectra of (i) 14L, (ii) 14Zn, (iii) 14CoCl, and (iv) 14YbOH in $CHCl_3$ at low temperature (77 K).

OEPErOH,[13] and TPPErOH.[13] The quantum yields ϕ_f of the latter group are 2.0×10^{-4}, 2.0×10^{-4}, and 2.1×10^{-4}, respectively.

The $S_1 \rightarrow S_0$ (Q band) quantum yield depends on the relative rates of the radiative process $S \rightarrow S_0$ and two radiationless processes $S_1 \rightsquigarrow S_0$ and $S_1 \rightsquigarrow T_n$. The fluorescence quantum yield of our complexes is <0.28. Thus, the excited state S_1 is

TABLE 4: Emission Spectral Data[a]

porphyrin	*T*/K	Q_1	ϕ_{f1}	τ_{f1}	Q_2	ϕ_{f2}	τ_{f2}	Q_3	ϕ_{f3}	τ_{f3}	T	ϕ_p	τ_p
14L	300	499	0.28	0.015	632	0.30	0.017	701	0.09	0.008			
	77	507	0.30	0.020	635	0.31	0.021	704	0.10	0.011			
14Zn(II)	300	492	0.25	0.022	641	0.25	0.021	702	0.06	0.012			
	77	507	0.26	0.028	635	0.28	0.026	703	0.08	0.015	724	0.07	26
14Co(III)Cl	300	515	0.20	0.017	635	0.22	0.018	702	0.06	0.009			
	77	517	0.24	0.021	635	0.24	0.022	704	0.07	0.011	725	0.06	22
14Yb(III)OH	300	521	0.23	0.028	637	0.25	0.032	704	0.08	0.014			
	77	529	0.26	0.034	641	0.27	0.036	704	0.09	0.016	720	0.07	32

[a] Q, fluorescent band (nm); T, phosphorescent band (nm); ϕ_f, fluorescence quantum yield; τ_f, fluorescence lifetime (ms).

primarily deactivated by radiationless decay. This indicates fairly certainly that the spin forbidden process $S_1 \rightsquigarrow T_n$ is the predominant one for radiationless deactivation of S_1 in porphyrin complexes. The quantum yield of the complexes at low temperature is higher than that at room temperature in the general case.

The $^2F_{5/2} \rightarrow {}^2F_{7/2}$ fluorescent emission of 14LYb(III)OH in the near-infrared range 970−1040 nm at 77 K was not measured. The fluorescent lifetimes of the Q bands for the complexes are in the region 0.017−0.028 ms at room temperature. This essentially agrees with the data in ref 14 but is higher than the data for ZnSPTBP.[12] When the chloroform solutions at 77 K were frozen, the quantum yield and fluorescent lifetimes of the ligand and complexes increased. The phosphorescent bands of the complexes at 77 K appear in the range 720−725 nm. Longo estimates the phosphorescent quantum yields of free base porphyrins to be <1% that of the porphyrin complexes. The phosphorescent emission of the complexes at 300 K and the ligand at 77 or 300 K did not appear.

There are similar results for the samples whose central ions are identical with those mentioned above.

The results of surface photovoltage and fluorescence spectroscopies show that the stronger the fluorescence intensity is, the weaker the surface photovoltage intensity is.

3. Conclusions

The first series of lanthanide(III) monobenzoporphyrin liquid crystals, TATBPYbOH, and relative transition metal benzoporphyrin liquid crystal compounds have been prepared. We have illustrated the application of cyclic voltammetry, fluorescence, and surface photovoltage spectroscopies in the analysis of hexagonar liquid crystals. Results indicate that these materials are mesogenic ones whose structures show the Col_h phase. The phase transition temperature regions of the liquid crystals (from C_6 to C_{16} derivatives) narrow gradually. The quantum yields and lifetimes of the complexes' $S_1 \rightarrow S_0$ emissions are consistent with the literature. The complexes at low temperature exhibit phosphorescence. The cyclic voltammetry contributes to the investigation of porphyrin liquid crystals and photochemical hole-burning materials. The results of SPS show that all samples are p-type semiconductors. With the rise of a positive electric field, the lifetime of the excited state was prolonged, leading to an increase in the SPV response. The electro-optical data storage effect of a liquid crystalline porphyrin may be related to the optoelectric properties of the resulted aggregates. The SPS techniques present a method for the investigation of functional semiconductor surface properties of photogenerated charge separation and charge transfer. These methods should be useful for the choice and applications of liquid crystalline materials.

4. Experimental Section

4.1. General Methods. ^{1}H NMR spectra were recorded on a Varian-Unity-400 (MHz) NMR spectrometer. Chemical shifts were reported on a δ-scale relative to tetramethylsilane (TMS). Elemental analyses were measured by a Perkin-Elmer 240 C auto elementary analyzer. Optical characterization was performed on a Leica DMLP polarizing microscope equipped with a Leica MPS30 Photoautomat along with a Linkam TM600 hot stage and controller. Transition temperatures and heats of fusion were determined at scan rates of 10 °C/min by differential scanning calorimetry using a METTLER TOLEDO DSC 821^e with a STAR^e thermal analysis system. Variable-temperature X-ray measurements were performed on a PW1700 X-ray diffractometry with Cu K radiation. UV/vis spectra were collected on a GBC UV−visible cintra 10/20/40 spectrometer. Infrared spectra were recorded on a Nicolet 5PC-FT-IR spectrometer in the region 200−4000 cm^{-1} using CsI pellets. Molar conductances at 25 °C were measured on a DDX-111A conductometer in DMF solution (1.00×10^{-3}). Redox potentials of the porphyrins (10^{-3} M) in dried DMF containing 0.1 M TBAP as a supporting electrolyte were determined at room temperature by cyclic voltammetry using a three-electrode system under deaerated conditions and a CHI 600A electrochemical analyzer. Platinum wires were used as working and counter electrodes. The reversibility of the electrochemical processes was evaluated by standard procedures, and all potentials were recorded against an Ag/Ag^+ reference electrode [0.01 M $AgNO_3$ in acetonitrile (CH_3CN) solution]. Fluorescence spectra were recorded with a SPEX Fluorolog-2T2 spectrofluorometer (450 W xenon lamp as the excitation source). Surface photovoltage spectroscopy was measured with a solid junction photovoltaic cell (ITO/sample/ITO) using a light source-monochromator-lock-in detection technique. All reagents and solvents were of commercial reagent grade and were used without further purification except DMF and CH_3CN. DMF was predried over activated 4 Å molecular sieves and vacuum distilled from calcium hydride (CaH_2) prior to use. The dry CH_3CN was obtained by redistillation from CaH_2 in a glovebox.

4.2. Preparation of Compounds. *14Zn.* A mixture of phthalimide (300 mg, 2.0 mmol) and zinc palmitic (700 mg, 1.2 mmol) was heated in a Mafu Stove at 350 °C for 25 min. The crude product was purified by column chromatography (silica gel, $CHCl_3$). The title compound was obtained as a green solid (429.4 mg, 0.3 mmol, yield 62%). ^{1}H NMR (400 MHz, $CDCl_3$) 7.43−7.48 (16H, isoindole), 0.87−0.90 (12H, CH_3), 1.26 (96H, CH_2), 1.60 (8H, CH_2); UV/vis ($CHCl_3$) λ_{max} ($10^{-4}\epsilon$, $M^{-1}\cdot cm^{-1}$) 430 (22.4), 578 (3.6), 629 (5.6); IR (CsI) 2924, 2851, 1325, 251 cm^{-1}. Anal. Calcd. for $ZnC_{92}H_{132}N_4$: C, 81.33; H, 9.72; N, 4.13. Found: C, 81.41; H, 9.64; N, 4.18. Molar conductance value (MCV) (DMF, 25 °C, $\Omega^{-1}\cdot cm^2\cdot mol^{-1}$) 5.4 (nonelectrolyte).[15]

14L. A total of 1.0×10^3 mg (0.7 mmol) of 14Zn was dissolved in 150.00 mL of chloroform and then 0.13 mL (1.6 mmol) of trifluoroacetic acid was added at room temperature. After stirring for 10 min, the reaction mixture was neutralized with an aqueous ammonia solution and then was washed with water. After evaporation of the solvent, the residue was purified by column chromatography (silica gel, $CHCl_3$). The title compound was obtained as a green solid (838.9 mg, 0.6 mmol, yield 88%).^{1}H NMR (400 MHz, $CDCl_3$) 7.43−7.48 (16H, isoindole), −1.13 (2H, N−H), 0.87−0.90 (12H, CH_3), 1.26 (96H, CH_2), 1.60 (8H, CH_2); UV/vis ($CHCl_3$) λ_{max} ($10^{-4}\epsilon$, $M^{-1}\cdot cm^{-1}$) 425 (22.6), 576 (3.2), 601 (3.6), 625 (5.7), 665 (2.9); IR (CsI) 3318, 2925, 2850, 1323 cm^{-1}. Anal. Calcd. for $C_{92}H_{134}N_4$: C, 85.32; H, 10.36; N, 4.33. Found: C, 85.33; H, 10.32; N, 4.28. MCV (DMF, 25 °C, $\Omega^{-1}\cdot cm^2\cdot mol^{-1}$) 0.9 (nonelectrolyte).

14YbOH. A mixture of 14L (300 mg, 0.23 mmol) and $YbCl_3$ (129.6 mg, 0.5 mmol) in imidazole (1.0×10^4 mg) was heated at 172 °C under N_2 for 10 min. The reaction mixture was cooled to 70 °C, and ethanol (10 mL) was added, and then chloroform (20 mL) was added. After the mixture was washed with water, 0.1% $AgNO_3$ was added until no AgCl precipitated. The mixture was purified by column chromatography (neutral aluminum oxide, ethanol). The title compound was obtained as a green solid (291.7 mg, 0.2 mmol, yield 85%).^{1}H NMR (400 MHz, $CDCl_3$) 7.43−7.48 (16H, isoindole), 0.87−0.90 (12H, CH_3), 1.26 (96H, CH_2), 1.60 (8H, CH_2), 0.50 (1H, OH); UV/vis ($CHCl_3$) λ_{max} ($10^{-4}\epsilon$, $M^{-1}\cdot cm^{-1}$) 438 (22.0), 578 (3.2), 631 (5.8); IR (CsI) 3423, 2925, 2850, 1326, 378 cm^{-1}. Anal. Calcd. for $YbC_{92}H_{133}N_4O$: C, 74.59; H, 8.90; N, 3.78. Found: C, 74.53; H, 8.94; N, 3.73. MCV (DMF, 25 °C, $\Omega^{-1}\cdot cm^2\cdot mol^{-1}$) 1.6 (nonelectrolyte).

14CoCl. 14CoCl was prepared by the reaction of 14L (300 mg, 0.23 mmol) with $CoCl_2\cdot 6H_2O$ (60.2 mg, 0.5 mmol) in a mixture of DMF (20 mL) and CH_2Cl_2 (20 mL) at refluxing temperature under N_2 for 5 min. The was CH_2Cl_2 removed by distillation. The mixture was washed with water and was filtered by suction and then was dried in vacuo. The crude product was purified by column chromatography (silica gel, $CHCl_3$). The title compound was obtained as a green solid (276.4 mg, 0.2 mmol, yield 86%). ^{1}H NMR (400 MHz, $CDCl_3$) 7.43−7.48 (16H, isoindole), 0.87−0.90 (12H, CH_3), 1.26 (96H, CH_2), 1.59 (8H, CH_2); UV/vis ($CHCl_3$) λ_{max} ($10^{-4}\epsilon$, $M^{-1}\cdot cm^{-1}$) 430 (22.1), 578 (3.18), 630 (5.7); IR (CsI) 2924, 2850, 1325, 322, 250 cm^{-1}. Anal. Calcd. for $CoC_{92}H_{132}N_4Cl$: C, 79.63; H, 9.52; N, 4.04. Found: C, 79.70; H, 9.58; N, 4.09. MCV (DMF, 25 °C, $\Omega^{-1}\cdot cm^2\cdot mol^{-1}$) 66.5 (1:1 type electrolyte).[15]

There are similar preparation methods and results for the samples whose central ions are identical with those mentioned above.

Acknowledgment. We thank the National Science Foundation of China for financial support of this work.

References and Notes

(1) Ramasseul, R.; Maldivi, P.; Marchon, J. C.; Taylor, M.; Guillon, D. *Liq. Cryst.* **1993**, *13*, 729.
(2) Chandrasekhar, S. *Liq. Cryst*. **1993**, *14*, 3.
(3) Liu, C.-Y.; Pan, H.-L.; Fox, M. A.; Bard, A. J. *Science* **1993**, *261*, 897.
(4) Levitsky, I. A.; Kishikawa, K.; Eichhorn, S. H.; Swager, T. M. *J. Am. Chem. Soc*. **2000**, *122*, 2474.
(5) Gatos, H. G.; Lagowski, J.; Banish, R. *Photogr. Sci. Eng.* **1982**, *26* (1), 42.
(6) Haudin, J. M. In *Optical Properties of Polymers*; Meeten, G. H., Ed.; Elsevier: New York, 1986; p 167.
(7) In some cases, disorder within the columns may produce a discotic lamellar phase instead. The reciprocal *d* spacings would then be 1:2.
(8) Felton, R. H.; Linschitz, H. *J. Am. Chem. Soc*. **1966**, *88*, 1113.
(9) Wang, D. J.; Liu, W.; Xiao, L. Z.; Li, T. J. *Chem. Bull.* **1989**, *10*, 32.
(10) Gregg, B. A.; Fox, M. A.; Bard, A. J. *J. Phys. Chem*. **1990**, *94*, 1586.
(11) Zalessky, I. E.; Kotlo, V. N.; Sevehenko; Solovgov, K. N.; Shkirman, S. F. *Dokl. Nauk, SSSR* **1974**, *21*, 312.
(12) Jiang, Z. X.; Chen, Z. P.; Wu, X. J. *Chin. Chem. Lett*. **1992**, *3* (8), 645.
(13) Kaizu, Y.; Asano, M.; Kobayashi, H. *J. Phys. Chem*. **1986**, *90*, 3906.
(14) Kachura, T. F.; Sevchenko, A. N.; Solovgov, K. N.; Tsvirko, M. P. *Dokl. Nauk, SSSR* **1974**, *217*, 1121.
(15) Geary, W. J. *Coord. Chem. Rev*. **1970**, *7*, 81.